Steady State Physical Modelling for Optimizing Capacitive Tactile Sensors Thermal Sensitivity

Rory Hampson, *Member, IEEE*, and Gordon Dobie

***Abstract*— Capacitive tactile pressure sensors are increasingly used in ergonomic testing and medical devices, specifically for human body measurement and characterising human interactions with their environment, where temperature coefficients are important considerations. New wearable and flexible sensor designs appear regularly in the literature however they rarely discuss why respective designs are improvements over predecessors, or any sensor performance optimisations for their intended applications. This lack of clear design rationale in the literature leads to inefficient design iterations and suboptimal sensor performance as designs are seemingly 'trial and errored'. This work analytically models the steady state mechanics of a simple commercial-off-the-shelf capacitive tactile sensor, SingleTact™ S15-4.5N, with nominal base temperature sensitivity of 0.2% FSR/°C, using multi-objective optimisation on the critical factors to minimise the temperature coefficient. This work investigates the governing factors for the temperature coefficients via sensitivity analysis on the experimentally validated model, providing novel design insight. By optimizing the design parameters within practical bounds, improvements of 16.16%, 16.47%, and 14.74%, can be achieved for the baseline, sensitivity, and linearity (steady state) temperature coefficients respectively. The model is shown to be useful in determining dominant factors controlling the steady state temperature coefficients as well as estimating sensitivity to manufacturing tolerances. This approach will be used on more complex designs in future to ensure optimal application performance, and assess the impact of manufacturing constraints on sensor performance to the benefit of manufacturers and end users alike.**

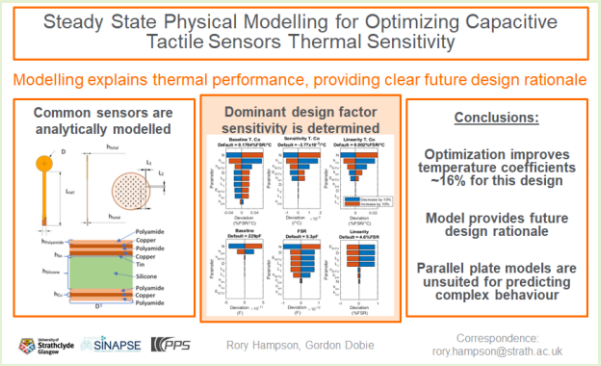

***Index Terms*—Capacitive Transducers, Mathematical Modelling, Optimization, Parametric Study, Performance Evaluation, Thermal Stability**

I. Introduction

CAPACITIVE tactile pressure sensors are a common method of measuring and quantifying tactile interactions, and are routinely employed in applications in contact with the human body [1], such as in medical imaging [2], [3], medical therapeutics [4]–[6], haptics and wearables [7], [8], and ergonomic testing [9] amongst others. These applications often involve large temperature variations and differentials during active operation, where performance is expected to be maintained throughout.

Capacitive pressure sensors, like all other tactile sensor types, have temperature coefficients that alter the performance of the sensor system under different environmental conditions. Researchers and designers frequently presenting novel designs and topologies in the literature with improved performance in some aspect than earlier works [10]–[13].

The critical problem is that discussion on why a particular design has better performance than another, or is as it is in isolation, is often superficial if present at all. It is also unknown whether authors have presented an optimal design based on their particular novel topologies for their intended applications, suggesting a lack of clear design rationale. Unclear rationale is a major driving force for slowed development and high costs.

Some authors have characterized and modelled various tactile sensor error sources for already produced sensors, usually for real-time compensation [14]–[16], but with little explanation of why it is so, and rarely any iterative design feedback. Others have begun to present clear modelling used to guide sensor design [12], however there remains a lack of clear understanding of why one design may be superior to another, resulting in potential trial and error for future designs.

Physical modelling has yielded understanding of parameters that govern effects such as hysteresis, and although the fundamental cause of temperature coefficients are known, there has been little work done on investigating the compounding effects of design parameters such as dimensions and material properties. This would be required to satisfactorily explain why performance is as it is, and what design choices are dominant in its sensitivity to temperature to guide future development.

This paper aims to fill this gap by using physical modelling to determine the dominant design factors controlling the temperature coefficients of tactile sensors, before optimizing to suggest practical design tweaks for better thermal performance.

This paper was submitted for review on 31/05/2023. This work was supported by the Scottish Imaging Network: A Platform for Scientific Excellence (SINAPSE) and PPS UK Limited.

Rory Hampson and Gordon Dobie are with Centre for Ultrasonic Engineering (CUE), University of Strathclyde, G1 1XW, GB. (Correspondence: rory.hampson@strath.ac.uk)

II. Scope and Structure of The Paper

This paper explores the governing factors that lead to the temperature coefficients present in tactile pressure sensors, by presenting an analytical physics based model of a common commercial-off-the-shelf (COTS) capacitive pressure sensor, focusing only on steady state effects such as baseline, sensitivity, and linearity temperature coefficients. This is then experimentally validated. The model is then analyzed to determine the optimality of the current design, before using optimization to propose design changes to reduce the temperature coefficient of similar sensors in future.

Section III introduces the method of operation of a basic capacitive pressure sensor. Section IV details driving factors for the temperature coefficient. Section V develops a physics based model for estimating the temperature coefficient based on sensor materials and geometry. Section VI shows the validation of the model experimentally. Sections VII and VIII deal with parameter sensitivity analysis and optimization of the design respectively. Section IX concludes with a discussion on the generalizability of this modelling approach, and feasibility of the optimized design.

III. General Capacitive Plate Pressure Sensor

The general equation for a parallel plate capacitor, shown in equation 1, describes how the capacitance 'C' between parallel plates is a function of the electrode area 'A', the permittivity of the dielectric material '$\varepsilon_0\varepsilon_R$', and the plate separation or dielectric thickness 'd'.

$$C = \frac{\varepsilon_0 \varepsilon_R A}{d} \tag{1}$$

This can be turned into a pressure sensitive capacitor by making the dielectric springy, such that it follows stress/strain relationship defined by the Young's Modulus of the dielectric material. Applying this principle to estimate the plate separation 'd' as a function of applied load, we get a general equation for a capacitive tactile sensor, as shown in equation 2. Here 'd_0' is the unloaded plate separation, 'E' is the material Young's modulus, and σ is the applied pressure. This obeys the normal stress sign convention of negative stress being compressive[1].

$$C = \frac{\varepsilon_0 \varepsilon_R A}{d_0\left(1 + \frac{\sigma}{E}\right)} \tag{2}$$

This model excludes the effect of capacitive fringing [17], but for the scale of sensors that shall be examined in this work it can be assumed to be negligible [18].

IV. Temperature Coefficient Driving Forces

One of the key effects of changing temperature on real materials is their thermal expansion, which is governed by the coefficient of linear expansion of the material and the temperature variance. Examining (2), it is clear that this will have an effect on the capacitance reading. Electrode expansion changes the value of 'A', and dielectric expansion changes the value of 'd_0' for example.

This is compounded when non homogeneous dielectrics, such as silicone beads, strips, or cones [1], [7], [19] are used. In this situation, thermal expansion of the silicone beads laterally changes the total area of silicone within the dielectric, which changes the ratio of silicone to air, which changes the average permittivity 'ε_R' of the dielectric media. This is shown in Figure 1. The problem is further compounded by thermal softening or stiffening of the dielectric, as many materials change their elastic properties in response to temperature [20]. This changes the value of 'E'. These effects can conflict, making it difficult to initially estimate sensor temperature coefficients.

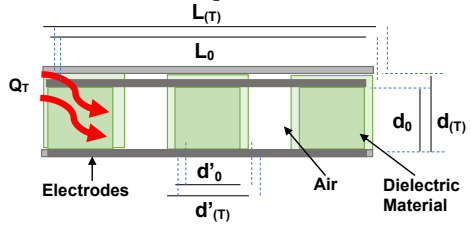

Figure 1 - Illustration of thermal behavior of parallel plate capacitors

V. Model Derivation

A. Sensor Architecture for Modelling

A common capacitive tactile sensor used in a wide array of applications (used/discussed in over 300 publications on Google Scholar as of 05/2023), that features a complex dielectric is the SingleTact™ (PPS UK Limited, GB). This is a suitable sensor for basing a general model on, as it is a parallel plate capacitor with a polymer/air dielectric similar to many others in the literature, and is commonly available. A diagram of the internal structure is shown in Figure 2, where the sensor face bears resemblance to the basic diagram shown in Figure 1.

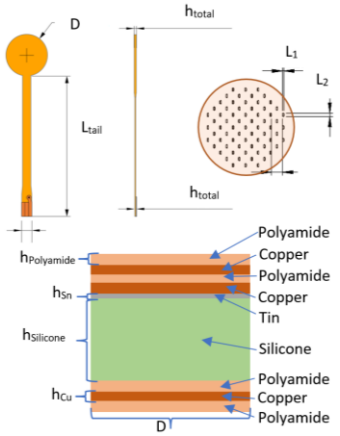

Figure 2 - Sensor Structure: Geometry, Layers, and Symbolic Terms

This sensor is made from several layers as shown, forming 3 distinct capacitors. One is largely pressure sensitive, the other 2 are relatively static, needed for shielding, or is the sensor tail. The dielectric is a mixture of room temperature vulcanizing (RTV) silicone beads, with the remainder being air, with a protective insulator covering one electrode. The other electrode is tin plated for protection. This sensor works using capacitance to the ground shield in a self-capacitance mode.

[1] It is common in sensor literature and datasheets to see stress that causes sensor compression to be displayed as positive, and tension to be negative to confuse the sign conventions, in which case the addition in (2) should become subtraction.

In general, an ideal sensor would have zero temperature drift, zero creep, zero hysteresis, and zero linearity error. A properly designed load cell, with perpendicular compensation, is close to having these properties. The SingleTact is further from ideal, but is useful due to its thin profile and flexibility, which load cells do not have. As such, these metrics must be carefully managed in order to maintain adequate sensor performance.

B. Thermal Effect on Materials

For each material layer, we can consider the thermal expansion radially and axially. For each layer 'i' the new dimensions 'L, h, D' of the layer in response to some change in temperature ΔT, can be calculated from (3), where K_{ELi} is the coefficient of linear thermal expansion of material 'i'.

$$L(T)_i = L_{0,i}\left(1 + K_{EL,i}\Delta T\right) \tag{3}$$

Which means that the area of the electrodes and area of each silicone bead will be expressed by (4).

$$A(T)_i = A_{0,i}\left(1 + K_{EL,i}\Delta T\right)^2 \tag{4}$$

As the dielectric is an air/silicone matrix, the total silicone area is given by (5), and the total air area in the dielectric will be given by (6), where N is the number of silicone beads.

$$A_{Silicone} = NA_{0,Silicone} \tag{5}$$

$$A(T)_{Air} = A(T)_{Electrode} - A(T)_{Silicone} \tag{6}$$

Finally, it is known that many real materials change elasticity with temperature, which can be expressed using (7), where K_{SE} is the coefficient of thermal softening.

$$E(T)_i = E_{0,i} + (K_{SE}\Delta T) \tag{7}$$

C. Thermal Electrode Deformation

Dissimilar bonded materials will be expanding at different rates, causing a mismatch strain that is known to cause warping, much like a bimetallic strip [21]. The mismatch strain ε_M between two dissimilar materials is given by (8), and the radius of curvature 'R' cause by this strain can be estimated using (9) [21] from the material elasticity 'E' and the thicknesses of each material 'h' calculated from (7) and (3) respectively.

$$\varepsilon_M = \left(K_{EL,1} - K_{EL,2}\right)\Delta T \tag{8}$$

$$R = \frac{E_1^2h_1^4 + 4E_1E_2h_1^3h_2 + 6E_1E_2h_1^2h_2^2 + 4E_1E_2h_1h_2^3 + E_2^2h_2^4}{6E_1E_2h_1h_2(h_1 + h_2)\varepsilon_M} \tag{9}$$

Only the centre electrode of this particular sensor will contribute significantly to curvature, with material 1 in (9) being tin plating, and material 2 being copper.

This radius is set at the centre of the electrode, and cannot be used to estimate a change in plate displacement by itself. We can calculate the radius on the surfaces using (10).

$$R_{Surface} = R \pm \frac{h_1 + h_2}{2} \tag{10}$$

D. Load Response on Plate Separation

The typical equation for Young's modulus applied in (2) assumes the dielectric is solid, and as such its effective area below the electrodes does not change. Whilst this is valid for a general material, it is not valid for the sensor as a system of materials. The reason can be observed in Figure 1, substituting thermal expansion for load, where an applied load causes the silicone beads to spread out (dictated by its Poisson ratio) and as such the stress in the material will be changing for a constant load on the electrodes. This must be taken into account when estimating the sensor load/displacement response.

Given that the area of a silicone bead is related to the axial strain 'ε_Z' by its Poisson ratio 'ν', as shown in (11), we can substitute (11) into the Young's modulus equation to obtain a nonlinear expression for the sensor strain in response to load, shown in (12), where F is the applied force on the electrode which can be solved by finding real roots. A and E are still functions of temperature from (4) and (7) respectively. $A_{Silicone}$ is the total designed silicone area, after thermal expansion.

$$A(T, \varepsilon_Z)_{Silicone} = A_{Silicone}(1 - \nu\varepsilon_Z)^2 \tag{11}$$

$$E\nu^2\varepsilon_Z^3 - 2E\nu\varepsilon_Z^2 - E\varepsilon_Z + \frac{F}{A_{Silicone}} = 0 \tag{12}$$

E. Combined Plate Separation Function

Following from (12), the expression for dielectric strain can be transferred into plate separation as shown in (13). Here $d(T)_{Silicone}$ is from (3) and ε_Z is from (12).

$$d_{Silicone} = d(T)_{Silicone}(1 + \varepsilon_Z) \tag{13}$$

The new thickness of the Kapton/polyamide layers is given by (14), as it is a simple solid. Here the area used to calculate σ is the electrode area and E is the elasticity of polyamide from (7).

$$d_{Polyamide} = d(T)_{Polyamide}\left(1 + \frac{\sigma}{E}\right) \tag{14}$$

The new average thickness of the main pressure sensitive layer is now expressed by (15).

$$d_{Average} = d_{Silicone} + d_{Polyamide} \tag{15}$$

This is an average as we must now bring back the curved centre electrode from Subsection C. The curvature of the electrode will settle at a line about the average separation such that the tensile forces balance the compressive forces in the dielectric. For a linear dielectric material, this line will be where the total volume of the curved dome electrode below some line α equals the total volume above this line. This is illustrated in Figure 3. The forces are small in comparison to the thermal stress, and so do not significantly affect R from (9).

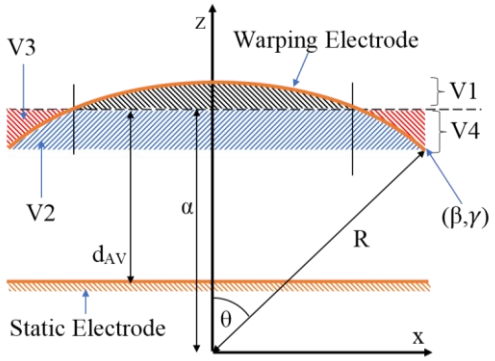

Figure 3 - Electrode warp visualization (exaggerated). The electrode will flex away from the surface with highest linear expansion. Settling about a plane where compressive and tensile strains are equal.

Using volumes of revolution to calculate volumes with respect to Figure 3, and the condition V1 = V3, we get (16) with γ and β defined as $R\cos(\theta)$ and $R\sin(\theta)$ respectively. This results in a polynomial in terms of α (17), which can be solved. This then yields the displacement function 'd' as shown in (18) which describes the plate separation at electrode location (x,y).

$$\pi\int_{\alpha}^{R} R^2 - z^2 dz = \pi\int_{\gamma}^{\alpha} \beta^2 dz - \pi\int_{\gamma}^{\alpha} R^2 - z^2 dz \quad (16)$$

$$\frac{2}{3}\alpha^3 - R^2(1+\cos(\theta)^2)\alpha + \frac{2}{3}R^3(1+\cos(\theta)^3) = 0 \quad (17)$$

$$d_{Silicone(x,y)} = d_{Silicone} + \alpha - \sqrt{R^2 - x^2 - y^2} \quad (18)$$

F. Capacitance Calculation

The total capacitance of the sensor is made up of 3 separate values: capacitance through the polyamide layer, capacitance through the RTV/Air/Polyamide layer, and the sensor tail.

The capacitance of the RTV/air/polyamide layer can be calculated by treating each of these dielectric media independently. The general equation for a non-parallel plate capacitor is given in (19), which reduces to (1) if the plates are parallel. The integral limits are adjusted to account for the circular electrode. Here 'r' is electrode radius.

$$C = \varepsilon_0\varepsilon_R\int_0^A \frac{dA}{d} = \varepsilon_0\varepsilon_R\int_{-r}^{r}\int_{-\sqrt{r^2-x^2}}^{\sqrt{r^2-x^2}} \frac{dy\,dx}{d} \quad (19)$$

We can use parallel dielectrics to determine the average value for ε_R for the RTV/air matrix as shown in (20).

$$\varepsilon_R = \frac{(\varepsilon_{Silicone}A_{Silicone} + \varepsilon_{Air}A_{Air})}{A_{Electrode}} \quad (20)$$

We can use the principle of stacked (series) dielectrics to estimate the capacitance through the combined RTV/air and Polyamide dielectric as shown in (21). C_{RTV} is given by (19) and $C_{Polymide}$ is given by (1), with respective values for d and ε_R.

$$C_{main} = \frac{C_{RTV}C_{Polyamide}}{C_{RTV} + C_{Polyamide}} \quad (21)$$

Additionally, the capacitance of the single polyamide layer ($C_{Backing}$) is calculated from recalculation of (19), with appropriate substitutions for 'd', and tail capacitance calculated from (22), yielding a final value for the sensor capacitance (23).

$$C_{Tail} = \frac{2\varepsilon_0\varepsilon_{Polyamide}L_{Tail}w_{trace}}{d_{polyamide}} \quad (22)$$

$$C_{Total} = C_{main} + C_{Backing} + C_{Tail} \quad (23)$$

G. Estimation of Temperature Coefficients

The linear thermal baseline shift can be determined in terms of % FSR/°C, where FSR is the full scale range of the sensor, using (24). K is the temperature coefficient, and $C_0(T)$ is the baseline capacitance at load = 0N at temperature difference T.

$$K_{Baseline} = \frac{C_0(T_1) - C_0(T_0)}{\Delta T} \quad (24)$$

Sensitivity to load (or scale factor) 'S' can be determined from (25), and temperature shift from (26), where $C_L(T)$ is the capacitance when loaded with 100%FSR at temperature T.

$$S(T) = \frac{C_L(T) - C_0(T)}{FSR} \quad (25)$$

$$K_{Sensitivity} = \frac{\left(\frac{S(T_1)}{S(T_0)} - 1\right)}{\Delta T} \quad (26)$$

Linearity is the max deviation of the capacitance with load (F) and temperature from ideal linearity (μ) as % FSR calculated using (27). This can then be turned into a temperature coefficient using (28). The baseline and sensitivity coefficients usually dominate this value, so this term is rarely seen in the academic or commercial literature.

$$\mu(T) = 100\frac{\max(|C(F,T)_{Observed} - C(F,T)_{Linear}|)}{FSR} \quad (27)$$

$$K_{Linearity} = \frac{\mu(T_1) - \mu(T_0)}{\Delta T} \quad (28)$$

VI. Experimental Validation

A. Methodology

In order to validate the model, the capacitance of the respective sensors must be measured w.r.t. load and temperature. This was over the range of load 0-4.5 N and temperature 20-50 °C, selected as a suitable range witnessed by close contact wearables. 3 identical sensors from different batches were measured to attempt to generalise the measurements. The sensor was fixed to a flat iron anvil with mass >> sensor, for thermal stability, using 3M 300LSE tape. A light rigid plastic disc with diameter D used to ensure uniform loading of the sensor face This is shown in Figure 4.

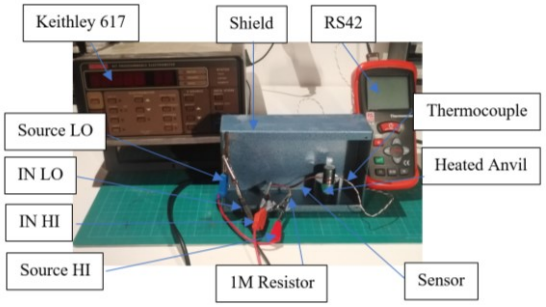

Figure 4 - Experimental Setup. The 617 is used as a voltage source, via the HI output, this connects to the sensor as shown via a 1M resistor. The charge accumulation is measured on the input HI line. Source and input LO lines are connected to a metal case around the heated sensor system. The shield is closed during measurements.

Capacitance of the sensor was measured using a Keithley 617 electrometer, using the manufacturer prescribed method. The charge integral error was captured for 5 seconds prior to each measurement, and subtracted out of the recorded value. For each temperature and load value, 5 capacitance measurements were made in quick succession and averaged. Loading was performed using iron weights, with total mass of 450 g to closely match the load rating of the sensor. Measurements were taken after 5 seconds of loading, to minimise the effect of sensor creep. Loads were removed during sensor heating and cooling.

Thermal cycling was performed by heating the iron anvil with warm air. The large thermal mass of the anvil maintains

thermal stability over the course of the measurements. Capacitance measurements, and loading, were performed when temperature measurements of the anvil, and loading plate, agreed within 1 °C. These were made using calibrated K-type thermocouples bonded to the sides of the respective objects and measured using an RS-42 thermometer. 10 total measurements of the temperature coefficients were made for 3 separate sensors, each trial consisting of a capacitance and temperature measurement at [20 °C, 0 N], [20 °C, 4.5 N], [50 °C, 0 N], and [50 °C, 4.5 N]. 10 minutes elapsed between measurements to allow for thermal stability and relaxation to be achieved.

B. Validation Results

The experimental validation results are shown in Figure 5, where experimental values for each temperature coefficient are compared to model predictions using varying material values and model complexities. Experimental temperature coefficients were calculated from (24) and (26), similar to the model.

It can be seen that the terms relating to warping of the electrode were necessary as without this a parallel plate model is a poor predictor of temperature coefficients. As there are large tolerances in the unit conversions of RTV silicone [20], [22] minor adjustments to the values of the K_{SE} - RTV and E_{RTV} were made from nominal values. Thus the model can predict temperature coefficients within experimental ranges.

This shows that the proposed model is a good predictor of the dominant temperature coefficients of the sensor, the baseline and FSR as shown in Figure 6 in line with the device datasheet [23], and can now be used to optimise the design.

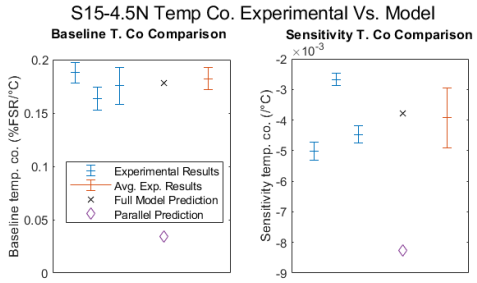

Figure 5 - Experimental model temperature response validation.

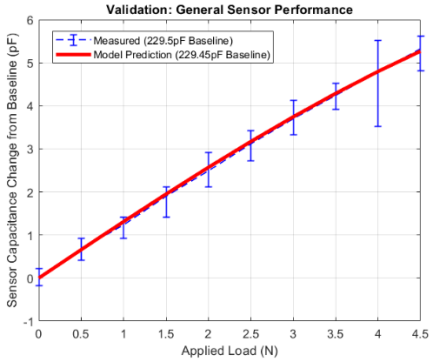

Figure 6 - General Sensor Simulation Validation. T = 20 °C, Baselines are subtracted to account for statistical differences

VII. Optimisation Design of Experiments

A. Experimental Constants

It is necessary to hold some parameters as constants during optimisation to reduce the parameter space. Some are fixed as they do not change within the work scope (e.g.: dimensions, metal properties). Others are fixed as there is insufficient data on their variability (e.g.: RTV coef. of thermal softening).

Table 1 - Constant Parameter Values

Constant	Value	Constant	Value
ε_0	8.854×10^{-12} F/m	ε_R - RTV	3.4
ε_R - Air	1	K_{EL} - RTV	200 ppm
E_{Cu}	117 GPa	K_{SE} - RTV	7.6 kPa/°C
K_{EL} - Cu	16.7 ppm	ν_{RTV}	0.49
E_{Sn}	41.6 GPa	ε_R - PA	3.4
K_{EL} - Sn	22.4 ppm	E_{PA}	2.7 GPa
L_{Tail}	40 mm	K_{EL} - PA	20 ppm
W_{Tail}	0.1 mm	-	-

B. Suitable Variables and Parameter Space

The values used in the model and the ranges of the parameter space is shown in Table 2. Some sensor dimensions, and RTV properties are continuously variable, and so ranges with even steps have been selected to cover a wide parameter space. Other parameters such as material thicknesses are variable by discrete values based on commonly available materials, and so these have limited ranges with only 2-3 values due to the availability of suitable materials such as copper weights and Polyamide sheets. Following the range selection, a Latin hypercube design was used to sample the parameter space for iterated local optimisations, allowing for efficient global optimisation.

Table 2 - Variables and Parameter Space

Parameter	Search Range	Variable Type
$\mathbf{E_{RTV}}$	0.7–1.5 MPa	Continuous
$\mathbf{h_{RTV}}$	150-210 µm	Continuous
$\mathbf{h_{Cu}}$	10-34 µm	Discrete
$\mathbf{h_{Sn}}$	0-9 µm	Discrete
$\mathbf{h_{PA}}$	10-75 µm	Discrete
$\mathbf{L_1}$	90-300 µm	Continuous
$\mathbf{L_2}$	300-760 µm	Continuous
N	50-97	Integer
D	6-15 mm	Continuous

C. Local Pre-Optimization Sensitivity Analysis

Prior to optimization, initial sensitivity analysis is performed on the variable parameters as shown in Figure 7.

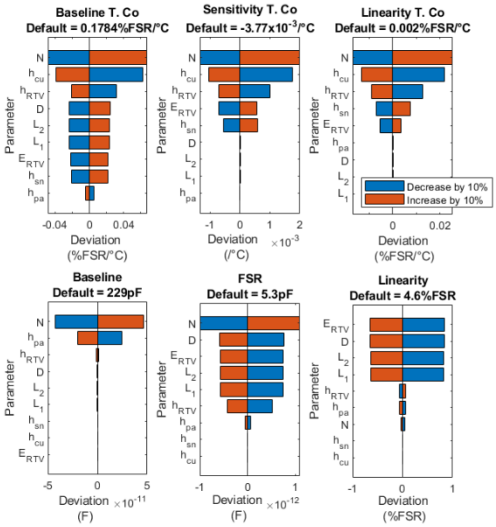

Figure 7 - Preoptimization Sensitivity Analysis

Here each parameter is modified by ±10% from its default value individually, with all others at their default value. The deviation in performance metrics are recorded and ranked for analysis.

For the 3 temperature coefficients, the dominant factors are consistently 'N', 'h_{cu}', and 'h_{RTV}'. Other factors become more important in the variability in the other metrics. It should be noted that the priorities of the parameters changes with each metric, and that some factors have negligible effect on some metrics whilst dominating others, such as 'E_{RTV}'.

VIII. Optimal Design Parameter Results

A. Optimization Results

There are 4 ways to optimize the sensor thermal performance. 3 permutations of optimizing 2 metrics at the expense of the third, and 1 method optimizing all 3 metrics simultaneously along a minimisation vector. It is the latter method that shall be adopted for this work. The Pareto solutions for each temperature coefficient are shown in Figure 8.

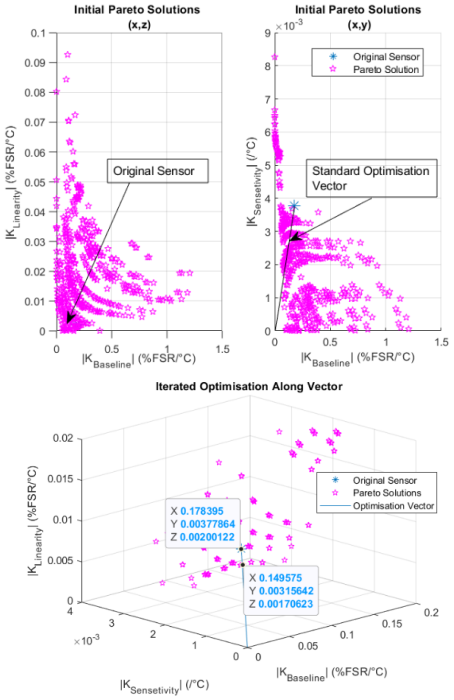

Figure 8 - Optimization Pareto Solutions and optimization vector

It can be seen that optimizing 2/3 parameters can be done effectively however the third parameter is always made worse than the original using this strategy. Only solutions maintaining useful Baseline, FSR, and linearity were retained. Optimizing along the optimization vector does reduce all temperature coefficients, however the gain is relatively small. This indicates the initial sensor design was close to optimal for its configuration. By adjusting the parameters within the design space, reductions in baseline, sensitivity, and linearity temperature coefficients of 16.16%, 16.47%, and 14.74% respectively were achieved as shown in Figure 8.

B. Optimized Design Parameters

The new design parameters from optimization are shown in Table 3, with comparison to the original values from Table 2. Manufacturing tolerances on these parameters are included for use in the discussion. The RTV layer is stiffer, corresponding to Shore 34A using Reuss approximation [22], thicker, with more but smaller dots. Sn and PA thickness remains consistent, Cu thickness is reduced to a rare but commercially available weight of 0.3 Oz/ft^2 and D is reduced to the same size as other sensors of this family. The increased cost of these different materials may limit the viability of implementation.

Table 3 - Optimized Sensor Parameters

Parameter	New Value	Mfr. Tolerance	Notes
E_{RTV}	1.43 MPa	±10%	Shore 34A
h_{RTV}	198 µm	±10 µm	-
h_{Cu}	10 µm	±10%	0.3 Oz/ft^2
h_{Sn}	5 µm	±10%	Standard
h_{PA}	25 µm	±10%	Standard
L_1	100 µm	±50 µm	-
L_2	583 µm	±50 µm	-
N	88	0	-
D	8 mm	±50 µm	-

C. Local Post-Optimization Sensitivity Analysis

Following optimization using the vector approach, local sensitivity analysis was performed again based on the optimised sensor parameters. This was done similarly to Section VII-C, as shown in Figure 9.

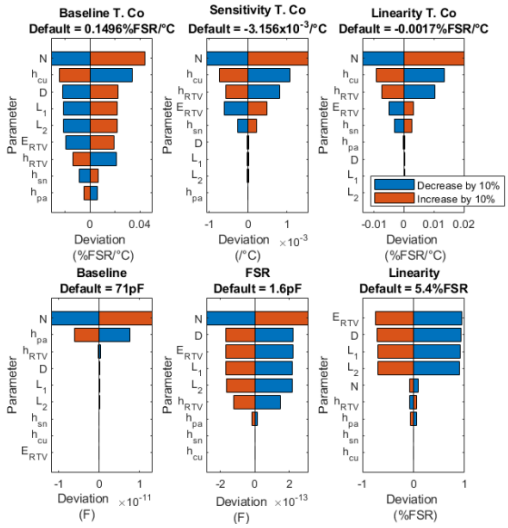

Figure 9 - Post Optimization Sensitivity Analysis

Interestingly, as shown in Figure 9, the top 2 dominant factors for each metric remains consistent with those from pre-optimization, shown in Figure 7, with the priority of the other factors changing in many cases. The sensitivity to local changes in each parameter is reduced significantly for all metrics except linearity, which is approximately the same as pre-optimisation.

IX. Discussion

A. Temperature Coefficient Optimization in Context

The modelling of the sensor structure in this work has allowed for the analysis of the dominant factors for the various temperature coefficients, and optimisation using the model has found that modest improvements in the order of 16% is possible

within practical manufacturing constraints. Although this is a good result, the performance improvement is modest as shown in Figure 10. A typical response plot pre and post optimization shows what this improvement means in terms of actual sensor output. Using a simple 2 point linear calibration in each case it can be seen that sensor output is less temperature dependent post optimisation, although this improvement is minor.

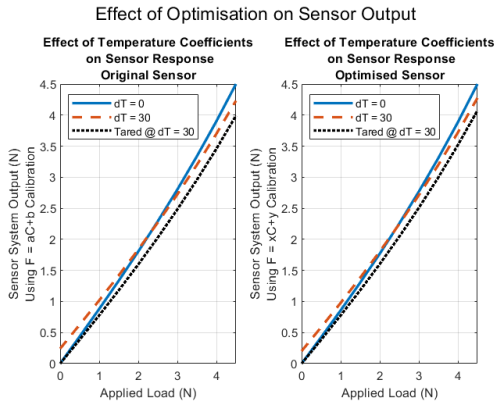

Figure 10 - Effect of Optimization on Sensor Performance. As can be seen, there is some improvement, despite the improvement on paper being significant (~16%), in context this has only minor impact.

B. Overall Post-Optimization Performance

The major reduction in baseline capacitance does not have an effect on sensor performance based on the current implementation of the CDC in the supplied electronics. The reduction in the FSR of the sensor will require a subsequent increase in gain in any measurement system to maintain digital counts or volts per unit load. This will subsequently have the effect of reducing the SNR of the sensor proportionally to the change in FSR. Although optimized sensor linearity is slightly worse than the original, the sign of the temperature coefficient has flipped, which makes the linearity better with temperature. This difference in linearity is minor compared to the FSR and so will have an insignificant effect on general performance.

Considering the sensitivities to parameter variations shown in Figure 7 and Figure 9, and tolerances shown in Table 3, it can be determined that batch reliability is improved with the optimized design, as sensitivity to variation in design parameters is reduced. This means that while thermal performance improves and general performance potentially reduces, the inter-sensor repeatability is greatly improved.

Finally, although switching RTV materials is relatively insignificant in terms of cost, the switching of copper weights represents a significant cost. This means that it is impractical to implement the optimised parameters from poor cost efficiency. The generalized modelling approach presented in this work can be applied to other sensor design topologies that may yield larger cost/benefit returns from optimization in future.

C. Model and Approach Limitations

The modelling presented in this work accurately predicts the major steady state temperature coefficients affecting all types of tactile sensor, as well as other loading metrics such as initial linearity and sensitivity. However there are several dynamic temperature related effects, and dynamic loading effects that this model does not yet feature including: thermal hysteresis, thermal change in creep/dynamic response, mechanical creep, material hysteresis, and dynamic heat transfer/temperature differentials. These thermal effects are expected to have an effect on performance, however they are complex to model physically and experimentally validate, beyond the scope of this work, and so steady state effects were the initial focus. Other RTV Silicone properties such as coef. of linear expansion and thermal softening vary with the base elasticity, but there is insufficient data to model this effect reliably.

This model lacks complexity to deal with shear loads supported by multi-directional sensors [24].

D. Generalization of the Model

The model can be generalized to support other homogeneous construction materials by making appropriate substitutions for the respective material properties, for example: substituting polyimide for PTFE, or copper electrodes with aluminium. Similarly, many sensors use solid silicone as dielectrics, rather than air/silicone matrix, which can be accommodated by setting the value of 'N' in Equation 5 to 1 and setting $A_{0,Silicone}$ to the desired value. Additionally, sensors using simple electrodes (as opposed to multi-metal) can be accommodated by omitting the warping terms introduced in Equations 16-18, and using the value of 'd' from Equation 15 alone to calculate the mutual capacitance. Other sensor configurations, such as mutual capacitance types [25] can be accommodated by considering the mutual and shield capacitances separately, although this adaptation does not hold for some implementations [13].

X. Conclusion and Future Work

This paper has presented and analytical model for a commonly used capacitive tactile pressure sensor, generalisable to a wide range of developing topologies, that accurately determines the steady state temperature coefficients of the sensor. This was used to determine the dominant factors controlling the sensor performance, namely: the electrode thickness and the compressible dielectric dimensions and stiffness. These parameters, among others, were optimised, with improvements in temperature coefficients in the order of 16% being possible. The knowledge of the governing factors from sensitivity analysis can be applied to new designs providing informed rationale for better design efficiency.

The main contributions of this work have been: An inspectable physical model describing the steady state temperature coefficients, the understanding that parallel plate assumptions are not necessarily appropriate for modelling thermal behaviours of nominally parallel plate sensors, and the sensitivity analysis of dominant design factors that can be applied in future designs.

The limitations of the model have been noted, and future work in this area will consist of performing similar analytical modelling of other sensor performance characteristics. This will lead to further understanding of what drives capacitive tactile sensor performance, and lead design efforts for generally applicable sensor systems in future.

XI. Conflict of Interest

Gordon Dobie is the managing director of PPS UK Limited, who are the suppliers of the sensors used for modelling and optimization in this work.

REFERENCES

[1] J. Xu, J. Pan, T. Cui, S. Zhang, Y. Yang, and T.-L. Ren, 'Recent Progress of Tactile and Force Sensors for Human–Machine Interaction', *Sensors*, vol. 23, no. 4, p. 1868, Feb. 2023, doi: 10.3390/s23041868.

[2] R. Hampson, G. West, and G. Dobie, 'Tactile, Orientation, and Optical Sensor Fusion for Tactile Breast Image Mosaicking', *IEEE SENSORS JOURNAL*, Jan. 2023, doi: 10.1109/JSEN.2023.3237906.

[3] A. Sarvazyan and V. Egorov, 'Mechanical imaging-a technology for 3-D visualization and characterization of soft tissue abnormalities: a review', *Current medical imaging reviews*, vol. 8, no. 1, pp. 64–73, 2012.

[4] R. Hampson, R. G. Anderson, and G. Dobie, 'Non-Invasive Radial Artery Blood Pressure Monitoring Using Error Compensated Tactile Sensors and Patient Specific Oscillometry', in *2022 44th Annual International Conference of the IEEE Engineering in Medicine & Biology Society (EMBC)*, Glasgow, Scotland, United Kingdom: IEEE, Jul. 2022, pp. 828–831. doi: 10.1109/EMBC48229.2022.9871598.

[5] A. Chandrasekhar, C.-S. Kim, M. Naji, K. Natarajan, J.-O. Hahn, and R. Mukkamala, 'Smartphone-based blood pressure monitoring via the oscillometric finger-pressing method', *Sci. Transl. Med.*, vol. 10, no. 431, p. eaap8674, Mar. 2018, doi: 10.1126/scitranslmed.aap8674.

[6] M. Yip, D. D. He, E. Winokur, A. G. Balderrama, R. Sheridan, and Hongshen Ma, 'A flexible pressure monitoring system for pressure ulcer prevention', in *2009 Annual International Conference of the IEEE Engineering in Medicine and Biology Society*, Minneapolis, MN: IEEE, Sep. 2009, pp. 1212–1215. doi: 10.1109/IEMBS.2009.5333964.

[7] Y. Kim, H. Yang, and J. H. Oh, 'Simple fabrication of highly sensitive capacitive pressure sensors using a porous dielectric layer with cone-shaped patterns', *Materials & Design*, vol. 197, p. 109203, Jan. 2021, doi: 10.1016/j.matdes.2020.109203.

[8] L. Viry *et al.*, 'Flexible Three-Axial Force Sensor for Soft and Highly Sensitive Artificial Touch', *Adv. Mater.*, vol. 26, no. 17, pp. 2659–2664, May 2014, doi: 10.1002/adma.201305064.

[9] G. Zhou, M.-L. Lu, and D. Yu, 'Investigating gripping force during lifting tasks using a pressure sensing glove system', *Applied Ergonomics*, vol. 107, p. 103917, Feb. 2023, doi: 10.1016/j.apergo.2022.103917.

[10] L. Ma *et al.*, 'Highly sensitive flexible capacitive pressure sensor with a broad linear response range and finite element analysis of micro-array electrode', *Journal of Materiomics*, vol. 6, no. 2, pp. 321–329, Jun. 2020, doi: 10.1016/j.jmat.2019.12.008.

[11] Y. Hara, K. Yoshida, A. Khosla, M. Kawakami, K. Hosoda, and H. Furukawa, 'Very Wide Sensing Range and Hysteresis Behaviors of Tactile Sensor Developed by Embedding Soft Ionic Gels in Soft Silicone Elastomers', *ECS J. Solid State Sci. Technol.*, vol. 9, no. 6, p. 061024, Aug. 2020, doi: 10.1149/2162-8777/aba913.

[12] J. Wu *et al.*, 'Rational design of flexible capacitive sensors with highly linear response over a broad pressure sensing range', *Nanoscale*, vol. 12, no. 41, pp. 21198–21206, 2020, doi: 10.1039/D0NR06386J.

[13] J.-C. Sicotte-Brisson, A. Bernier, J. Kwiatkowski, and V. Duchaine, 'Capacitive Tactile Sensor Using Mutual Capacitance Sensing Method for Increased Resolution', in *2022 International Conference on Robotics and Automation (ICRA)*, Philadelphia, PA, USA: IEEE, May 2022, pp. 10788–10794. doi: 10.1109/ICRA46639.2022.9811696.

[14] J. Sánchez-Durán, F. Vidal-Verdú, Ó. Oballe-Peinado, J. Castellanos-Ramos, and J. Hidalgo-López, 'A New Model Based on Adaptation of the External Loop to Compensate the Hysteresis of Tactile Sensors', *Sensors*, vol. 15, no. 10, pp. 26170–26197, Oct. 2015, doi: 10.3390/s151026170.

[15] R. Koike, S. Sakaino, and T. Tsuji, 'Hysteresis Compensation in Force/Torque Sensors Using Time Series Information', *Sensors*, vol. 19, no. 19, p. 4259, Sep. 2019, doi: 10.3390/s19194259.

[16] M. Baghelani, A. Hosseini-Sianaki, Z. Behzadi, and A. Mirabdolah Lavasani, 'Simulation of capacitive pressure sensor based on microelectromechanical systems technology', *Proceedings of the Institution of Mechanical Engineers, Part C: Journal of Mechanical Engineering Science*, vol. 232, no. 9, pp. 1538–1546, May 2018, doi: 10.1177/0954406217706095.

[17] M. Hosseini, G. Zhu, and Y.-A. Peter, 'A new formulation of fringing capacitance and its application to the control of parallel-plate electrostatic micro actuators', *Analog Integr Circ Sig Process*, vol. 53, no. 2–3, pp. 119–128, Oct. 2007, doi: 10.1007/s10470-007-9067-3.

[18] X. Chen, Z. Zhang, S. Yu, and T.-G. Zsurzsan, 'Fringing Effect Analysis of Parallel Plate Capacitors for Capacitive Power Transfer Application', in *2019 IEEE 4th International Future Energy Electronics Conference (IFEEC)*, Singapore, Singapore: IEEE, Nov. 2019, pp. 1–5. doi: 10.1109/IFEEC47410.2019.9015111.

[19] Y. Mu *et al.*, 'All-printed flexible capacitive array tactile force sensors with tunable sensitivity and low crosstalk for micro motion detection', *Sensors and Actuators A: Physical*, vol. 356, p. 114337, Jun. 2023, doi: 10.1016/j.sna.2023.114337.

[20] T. M. Mower, 'Thermomechanical behavior of aerospace-grade RTV (silicone adhesive)', *International Journal of Adhesion and Adhesives*, vol. 87, pp. 64–72, Dec. 2018, doi: 10.1016/j.ijadhadh.2018.08.009.

[21] G. D. Angel and G. Haritos, 'An Immediate Formula for the Radius of Curvature of A Bimetallic Strip', *International Journal of Engineering Research*, vol. 2, no. 12, 2013.

[22] K. Larson, 'Can You Estimate Modulus From Durometer Hardness for Silicones?', *DOW White Paper*, 2019, Accessed: Feb. 18, 2023. [Online]. Available: https://www.dow.com/content/dam/dcc/documents/en-us/tech-art/11/11-37/11-3716-01-durometer-hardness-for-silicones.pdf

[23] PPS UK Limited, 'SingleTact Datasheet'. PPS UK Limited, 2023. Accessed: May 25, 2023. [Online]. Available: https://www.singletact.com/SingleTact_Datasheet.pdf

[24] Y. Zhu, X. Chen, K. Chu, X. Wang, Z. Hu, and H. Su, 'Carbon Black/PDMS Based Flexible Capacitive Tactile Sensor for Multi-Directional Force Sensing', *Sensors*, vol. 22, no. 2, p. 628, Jan. 2022, doi: 10.3390/s22020628.

[25] S. Akbarzadeh *et al.*, 'A Simple Fabrication, Low Noise, Capacitive Tactile Sensor for Use in Inexpensive and Smart Healthcare Systems', *IEEE Sensors J.*, vol. 22, no. 9, pp. 9069–9077, May 2022, doi: 10.1109/JSEN.2022.3159610.

AUTHOR BIOGRAPHIES

Rory Hampson received the PhD and MEng degrees from the University of Strathclyde, Glasgow, U.K., in 2021 and 2017 respectively. He is currently a researcher in the Department of Electronic and Electrical Engineering at the University of Strathclyde. His current work focusses on tactile imaging for breast cancer diagnosis, medical decision making based on tactile sensor technology, and automated inspection robots. His research interests are Medical Imaging, Inertial Guidance and Control, Nuclear Inspection, and Engineering Sustainable Development.

Gordon Dobie received the Ph.D. degree in electrical and mechanical engineering from the University of Strathclyde with a focus on development of reconfigurable non-contact inspection system. He is currently a Reader with the department of Electronic and Electrical Engineering, University of Strathclyde. He is currently with CUE, where he is involved in automated ultrasonic inspection of complex geometries. His primary research interests are ultrasonics, NDE, automation, robotics, signal processing, computer vision and embedded systems.